International Journal of Multiphase Flow 35 (2009) 1138–1148

Contents lists available at ScienceDirect

International Journal of Multiphase Flow

journal homepage: www.elsevier.com/locate/ijmulflow

Unified macro-to-microscale method to predict two-phase frictional pressure drops of annular flows

Andrea Cioncolini [a,1], John R. Thome [a,*], Carlo Lombardi [b,2]

[a] Heat and Mass Transfer Laboratory, École Polytechnique Fédérale de Lausanne, EPFL-STI-IGM-LTCM, Station 9, 1015 Lausanne, Switzerland
[b] Department of Nuclear Engineering, Politecnico di Milano, via Ponzio 34/3, 20133 Milano, Italy

ARTICLE INFO

Article history:
Received 27 April 2009
Received in revised form 29 June 2009
Accepted 16 July 2009
Available online 19 July 2009

Keywords:
Annular two-phase flow
Pressure gradient
Pressure drop
Microchannels

ABSTRACT

The study considers the prediction of pressure gradients in adiabatic gas–liquid annular two-phase flow in the macro-to-microscale range. Twenty-four empirical correlations have been tested against an experimental data bank drawn together in this study containing 3908 points for eight different gas–liquid combinations and 22 different tube diameters, covering microscale and macroscale channels from 0.517 to 31.7 mm in diameter. The correlations of Lombardi, Friedel and Baroczy-Chisholm were found to be the best existing methods when considering macroscale data only, while the microscale database was best predicted by the correlations of Lombardi, Müller-Steinhagen and Heck and the homogeneous model with the two-phase viscosity defined according to Cicchitti. A new correlating approach based on the vapor core Weber number, capable of providing physical insight into the flow, was proposed and worked better than any of the existing methods for the macroscale database. This new macroscale method was then extended to cover microscale conditions, resulting in one unified method for predicting annular flows from the macroscale to the microscale covering both laminar and turbulent liquid films. The macroscale method optimized for microchannels worked better than any of the other methods considered.

1. Introduction

Annular two-phase flow is one of the most frequently observed flow patterns in practical applications involving gas–liquid two-phase flow, such as steam–water systems, liquid film evaporators, air-conditioning systems, two-phase flow heat exchangers and gas–liquid transportation systems. Annular flow is characterized by the presence of a continuous liquid film flowing on the channel wall, surrounding a central gas core laden with entrained liquid droplets. Since accurate predictions of the pressure gradient are critical for an energy efficient design of any two-phase flow system, the subject of two-phase pressure drops has been extensively investigated in the last decades and numerous empirical correlations are available. With annular two-phase flow, in particular, besides its relevance for design applications, the prediction of the pressure gradient is also of interest for the modeling of such flows to obtain relevant flow parameters such as the liquid film thickness and the void fraction. Such annular flow models typically require as input the wall shear stress, and thus an accurate two-phase pressure drop method.

The purpose of the present study is to first assess the accuracy of leading empirical pressure drop correlations, focusing in particular on adiabatic annular two-phase flows. An experimental pressure drop database, containing 3908 points for annular two-phase flow covering eight different gas–liquid combinations and 22 tube diameters, ranging from the micro to macroscale, has been collected from the open literature. The database is used to assess the predictive capability of 24 empirical correlations: 11 different implementations of the homogeneous model, nine general purpose empirical correlations and four more empirical methods specifically designed for microchannels. Finally, a new correlating approach based on dimensional analysis and capable of providing a physical insight that empirical correlations typically lack is proposed, covering the entire range from macroscale to microscale and both laminar and turbulent liquid films.

2. Experimental database description

The main details regarding the experimental pressure drop database collected from the open literature are summarized in Table 1. All data refer to adiabatic gas–liquid (or vapor–liquid) annular two-phase flow through circular pipes. The collected data cover eight different gas–liquid combinations, including both single-component saturated fluids such as water–steam and refrigerants R134a and R245fa and two-component fluids, such as water–air,

* Corresponding author. Tel.: +41 21 693 5981; fax: +41 21 693 5960.
E-mail addresses: andrea.cioncolini@epfl.ch (A. Cioncolini), john.thome@epfl.ch (J.R. Thome), carlo.lombardi@fastwebnet.it (C. Lombardi).
[1] Tel.: +41 21 693 5984; fax: +41 21 693 5960.
[2] Tel.: +39 02 2399 6332; fax: +39 02 2399 6309.

0301-9322/$ - see front matter © 2009 Elsevier Ltd. All rights reserved.
doi:10.1016/j.ijmultiphaseflow.2009.07.005

Table 1
Experimental annular flow data bank.

Reference	Fluids	d (mm)	Orientation, Tube material	P (MPa)	G (kgm^{-2} s^{-1})	x	Classification[a] Marker[b]	L/d[c]	No. points
CISE saturated (Silvestri at al., 1963; Gaspari et al., 1964)	H_2O–steam	4.90;4.99;5.00; 5.04;5.08;5.20; 6.30;8.07;8.20; 9.18;10.1;15.2; 24.9	↑ Stainless steel	2.0–9.4	497–4398	0.02–0.87	M-△	8–510	1501
CISE 2 component (Silvestri at al. 1963; Adorni et al., 1963; Casagrande et al., 1963; Cravarolo et al., 1964)	H_2O–argon H_2O–nitrogen Alcohol–argon H_2O–alcohol–argon	15.1;25.0	↑ Perspex	0.3–2.4	255–3420	0.04–0.84	M-○	20–199	1529
Water–Air (Anderson and Mantzouranis, 1960; Gill et al., 1964, 1965; Shearer and Nedderman, 1965; Willis, 1965)	H_2O–air	10.8;12.7; 15.9;31.7	↑ Perspex glass	0.1–0.2	39.4–1391	0.01–0.97	M-□	9–133	296
LTCM (Revellin, 2005; Revellin and Thome, 2007; Consolini, 2008)	R134a R245fa	0.517;0.803; 1.03	→ Glass	0.2–0.9	184–1694	0.09–0.95	μ-◇	24–48	582

[a] M, macroscale, μ, microscale.
[b] Marker used in figures.
[c] Distance of test section inlet from mixer (two component flows) or preheater (saturated flows).

water–argon, water–nitrogen and ethyl alcohol–argon. In addition, a mixture of ethyl alcohol and water, with the ethyl alcohol concentration varying from 5% to 90% in weight and tested with argon is included. The experimental data cover 22 different values of tube diameter, ranging from 0.517 to 31.7 mm and spanning from micro to macroscale. In particular, in the present study the data are classified as microscale or macroscale according to the criterion proposed by Kandlikar (2002) that fixes the macro-to-micro diameter threshold below which miniaturization effects on two-phase flow become significant at 3 mm. Accordingly, all the refrigerant data are classified as microscale, while all other data are classified as macroscale. It is worth highlighting, however, that Kandlikar's criterion is only preliminary, as the macro-to-microscale transition in two-phase flow is still an area of active research. Notably, all the macroscale data are for vertical upflow, while the microscale data refer to horizontal flow.

All macroscale data for gas–liquid flows and microscale data for refrigerants have been obtained with transparent test sections to allow the visual detection of the flow regime. All these data cover adiabatic annular flow only, without any contamination of data from other flow regimes. Macroscale data for adiabatic water-steam, on the other hand, have been obtained with stainless steel test sections and cover all flow regimes, not only annular flow. Therefore, these data have been analyzed with the flow map of Hewitt and Roberts (1969) and the data regarding annular flow have been segregated for use here, as indicated in Fig. 1. Since flow map transition boundary lines are known to be approximate and actually specify the middle of a transition between two regimes, test conditions that are predicted to be annular flow but that fall very close to the boundary lines have also been excluded. Out of the original CISE saturated database containing 1581 points, 1501 points are predicted to be annular flow, as indicated in Table 1, corresponding to ~95% of the original data. This further highlights the predominance of the annular flow regime in practical applications. The flow map of Hewitt and Roberts is valid for vertical, adiabatic upflow and is based on observations for low pressure air–water and high pressure steam–water flows in 10–30 mm diameter tubes, so that its use appears appropriate in the present context. As a further check, as shown in Fig. 2 (the markers used in the figures in the present study are described in Table 1), the flow map of Hewitt and Roberts is also used to analyze the rest of the macroscale database, which is known to cover annular flow only, yielding quite satisfactory results.

Since annular two-phase flow can be quite slow in reaching fully developed flow conditions and some inlet effects can be present up to 100–300 tube diameters from the inlet (Wolf et al., 2001), some data might be affected by a residual dependence on inlet conditions. Inlet effects, however, are not considered in the present study and no data were excluded since no viable criterion is apparently available.

As pressure gradient values can be particularly high with small diameter tubes, the flashing of the two-phase flow through the test section can become significant with microchannels. In the present study, in particular, the biasing of the microscale data from excessive flashing is prevented by excluding from the database all the data characterized by a vapor quality variation through the test section greater than 10% (i.e., if the vapor quality at the inlet of the test section is 0.50, then the experimental point is excluded from the database if the vapor quality at the test section outlet is predicted to be above 0.55). Out of the original LTCM microscale database containing 1166 points, 582 points are predicted to satisfy the above limiting condition on flashing, as indicated in Table 1.

3. Empirical correlations

In this study, 24 empirical correlations of frequent use in two-phase flow design applications are considered: 11 different implementations of the homogeneous model (with two-phase viscosity defined according to McAdams et al., 1942, Cicchitti et al., 1960, Dukler et al., 1964, Owens, 1961, Beattie and Whalley, 1982, Davidson et al., 1943, Garcia et al., 2003 and Awad and Muzychka, 2008), plus the macroscale correlations of Lockhart and Martinelli (1949), Martinelli and Nelson (1948), Baroczy (1966) and Chisholm (1973), Friedel (1979), Theissing (Stephan, 1992), Lombardi (Lombardi and Carsana, 1992), Müller-Steinhagen and Heck (1986), Chawla (Stephan, 1992) and Shannak (2008). Besides, the microscale methods proposed by Mishima and Hibiki (1996), Zhang and Mishima (Zhang, 2006), Sun and Mishima (2009) and Tran (Tran et al., 2000) are also considered.

Further details on these correlations and their implementation can be found in the Electronic Annex 1 in the online version of this article.

4. Results

The comparison of the measured pressure drop data versus these empirical correlation predictions is presented in the figures

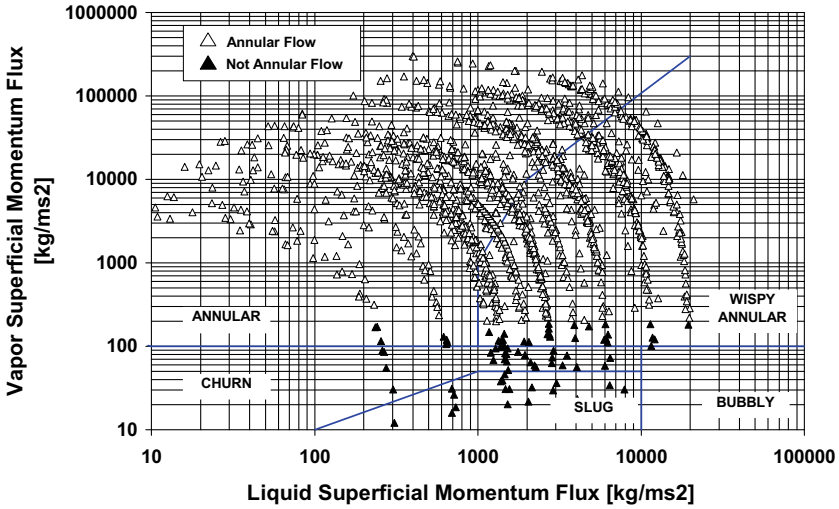

Fig. 1. Flow regime predictions for CISE saturated data.

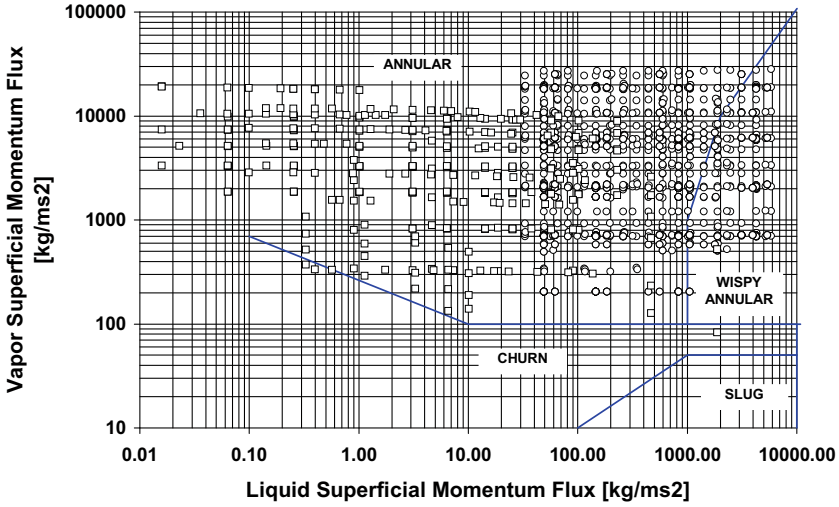

Fig. 2. Flow regime predictions for CISE 2 component and water–air data.

included in the Electronic Annex 2 in the online version of this article, where the measured pressure gradients are compared with predicted ones, while the statistical comparisons between measured data and predictions are reported in Tables 2 and 3 for the macroscale and the microscale data, respectively. Both the homogeneous model and the correlation of Lombardi predict the total pressure gradient, allowing a direct comparison of the predictions with the total pressure drop data, as shown in Figs. 1–11 and 17 in the Electronic Annex 2 in the online version of this article. The other empirical correlations considered, however, only predict the frictional component of the pressure gradient. The rationale behind this is that in most two-phase flow systems the frictional component of the total pressure gradient is largely predominant, while it is left to the user to choose a void fraction equation to estimate the accelerative and gravitational components. In this study, in particular, the frictional component of the total pressure gradient is calculated from the linear momentum conservation equation for the total flow, which for steady-state and fully-developed annular two-phase flow is as follows:

$$-\left(\frac{dP}{dz}\right)_{tpf-t} = \frac{4\tau_w}{d} + G^2\frac{d}{dz}\left[\frac{x^2}{\rho_g\varepsilon} + \frac{e^2(1-x)^2}{\rho_l\gamma(1-\varepsilon)} + \frac{(1-e)^2(1-x)^2}{\rho_l(1-\gamma)(1-\varepsilon)}\right] + [\rho_l(1-\varepsilon) + \rho_g\varepsilon]g\sin(\theta) \quad (1)$$

The three terms appearing on the right-hand side of Eq. (1) represent the frictional, the acceleration and the gravitational components of the total pressure gradient, respectively, τ_w is the wall shear stress and e is the fraction of liquid entrained as droplets in the gas core. As schematically indicated in Fig. 3, ε is the void fraction, which represents the fraction of the channel cross sectional area occupied by the gas phase, while γ is the liquid droplet hold-up, representing the fraction of the liquid phase cross sectional area occupied by the entrained droplets.

If the wall shear stress τ_w is assumed to be constant along the channel, while the densities ρ_l and ρ_g and the void fraction ε are assumed to vary linearly along the channel, which is considered to be acceptable to capture the small variations in these flow parameters induced by the pressure reduction along the channel, then Eq. (1) can be integrated to provide the following estimate of the frictional component of the pressure gradient:

$$\left(\frac{dP}{dz}\right)_{tpf-f} = \frac{4\tau_w}{d} = \frac{|\Delta P|}{L_{dp}} - \frac{G^2}{L_{dp}}(\Phi_{out} - \Phi_{in}) - g\sin(\theta)\Psi \quad (2)$$

where ΔP is the measured total pressure drop and L_{dp} is the distance between the pressure taps, while the parameters Φ and Ψ are as follows:

Table 2
Statistical comparison between macroscale experimental data and correlations.

	(1)	(2)	(3)	(4)	(5)
Homogeneous-McAdams	35.0	33.2	18.0	39.5	74.6
Homogeneous-Cicchitti	25.7	14.5	28.2	61.1	95.9
Homogeneous-Dukler	37.0	35.6	13.9	32.6	73.9
Homogeneous-Owens	26.0	4.5	30.3	70.4	92.8
Homogeneous-Beattie and Whalley	31.7	28.2	21.0	43.5	83.6
Homogeneous-Davidson	2730	−2728	22.6	35.4	48.7
Homogeneous-Garcia	41.5	40.1	6.9	24.7	64.4
Homogeneous-Awad and Muzychka No. 1	26.2	16.6	28.0	59.0	95.7
Homogeneous-Awad and Muzychka No. 2	31.4	28.3	22.2	47.4	80.8
Homogeneous-Awad and Muzychka No. 3	27.3	19.9	26.1	57.6	91.8
Homogeneous-Awad and Muzychka No. 4	27.5	21.1	26.3	54.7	93.7
Lockhart and Martinelli	96.0	−89.2	14.2	25.3	36.4
Martinelli and Nelson	240	−240	6.4	14.3	28.4
Baroczy-Chisholm	25.0	8.7	39.3	65.6	90.4
Friedel	21.9	6.7	38.8	72.7	96.4
Theissing	27.1	15.6	28.0	58.2	91.7
Lombardi	15.9	−10.1	61.8	89.4	95.8
Müller-Steinhagen and Heck	28.2	11.8	30.3	52.9	88.6
Chawla	48.7	48.4	5.3	18.2	48.3
Shannak	29.7	23.3	25.1	52.5	83.0
Mishima and Hibiki	91.7	−86.9	14.6	25.9	36.4
Zhang-Mishima	80.8	−74.8	15.6	28.8	41.4
Sun-Mishima	29.1	15.6	27.2	56.0	92.8
Tran	53.8	−30.4	21.8	42.0	63.8
Present study, Eqs. (30) and (31)	13.1	−2.4	69.7	92.7	97.1

(1) Mean absolute percentage error (%) $\frac{100}{n}\sum_1^n \frac{|(dP/dz)_{exp}-(dP/dz)_{cal}|}{(dP/dz)_{exp}}$.
(2) Mean percentage error (%) $\frac{100}{n}\sum_1^n \frac{(dP/dz)_{exp}-(dP/dz)_{cal}}{(dP/dz)_{exp}}$.
(3) Percentage of experimental data within ±15%.
(4) Percentage of experimental data within ±30%.
(5) Percentage of experimental data within ±50%.

Table 3
Statistical comparison between microscale experimental data and correlations.

	(1)	(2)	(3)	(4)	(5)
Homogeneous-McAdams	43.6	43.3	4.5	9.4	75.4
Homogeneous-Cicchitti	26.6	16.5	18.2	71.8	95.4
Homogeneous-Dukler	47.7	47.7	1.7	7.7	53.3
Homogeneous-Owens	40.0	−8.4	27.0	67.0	85.0
Homogeneous-Beattie and Whalley	39.2	38.9	4.5	15.8	88.3
Homogeneous-Davidson	3285	−3284	1.2	3.9	5.5
Homogeneous-Garcia	52.8	52.8	0.2	2.1	24.7
Homogeneous-Awad and Muzychka No. 1	27.8	21.0	15.5	62.0	96.2
Homogeneous-Awad and Muzychka No. 2	36.8	35.3	5.0	22.0	91.4
Homogeneous-Awad and Muzychka No. 3	30.0	25.2	10.3	49.5	97.1
Homogeneous-Awad and Muzychka No. 4	30.1	27.8	12.5	38.7	96.9
Lockhart and Martinelli	41.3	−36.3	27.0	52.6	63.9
Martinelli and Nelson	683	−683	0.0	0.0	0.0
Baroczy-Chisholm	32.6	−8.3	31.1	73.4	86.4
Friedel	28.0	10.2	22.7	69.9	90.9
Theissing	31.9	28.0	9.8	38.0	95.2
Lombardi	18.2	−5.2	58.9	87.5	94.0
Müller-Steinhagen and Heck	24.2	18.5	26.3	67.2	97.8
Chawla	51.8	51.7	1.7	7.4	34.5
Shannak	38.3	37.7	3.9	17.9	89.0
Mishima and Hibiki	47.2	47.1	1.5	9.3	51.7
Zhang-Mishima	39.8	39.7	2.4	16.0	83.3
Sun-Mishima	28.8	22.1	16.3	51.4	97.1
Tran	185	−185	0.5	3.4	6.9
Present study, Eqs. (30) and (31)	28.8	10.9	22.8	51.2	92.1
Present study, Eqs. (31) and (34)	13.1	9.2	62.2	97.8	100.0

(1) Mean absolute percentage error (%) $\frac{100}{n}\sum_1^n \frac{|(dP/dz)_{exp}-(dP/dz)_{cal}|}{(dP/dz)_{exp}}$.
(2) Mean percentage error (%) $\frac{100}{n}\sum_1^n \frac{(dP/dz)_{exp}-(dP/dz)_{cal}}{(dP/dz)_{exp}}$.
(3) Percentage of experimental data within ±15%.
(4) Percentage of experimental data within ±30%.
(5) Percentage of experimental data within ±50%.

$$\Phi_{in} = \frac{e_{in}^2(1-x_{in})^2}{\rho_{lin}\gamma_{in}(1-\varepsilon_{in})} + \frac{(1-e_{in})^2(1-x_{in})^2}{\rho_{lin}(1-\gamma_{in})(1-\varepsilon_{in})} + \frac{x_{in}^2}{\rho_{gin}\varepsilon_{in}} \tag{3}$$

$$\Phi_{out} = \frac{e_{out}^2(1-x_{out})^2}{\rho_{lout}\gamma_{out}(1-\varepsilon_{out})} + \frac{(1-e_{out})^2(1-x_{out})^2}{\rho_{lout}(1-\gamma_{out})(1-\varepsilon_{out})} + \frac{x_{out}^2}{\rho_{gout}\varepsilon_{out}} \tag{4}$$

$$\Psi = \frac{1}{3}\Delta\varepsilon(\Delta\rho_g - \Delta\rho_l) + \frac{1}{2}[\Delta\varepsilon(\rho_{gin} - \rho_{lin}) + (1-\varepsilon_{in})\Delta\rho_l + \varepsilon_{in}\Delta\rho_g] + \rho_{lin}(1-\varepsilon_{in}) + \rho_{gin}\varepsilon_{in} \tag{5}$$

$$\Delta\rho_l = \rho_{lout} - \rho_{lin}, \quad \Delta\rho_g = \rho_{gout} - \rho_{gin}, \quad \Delta\varepsilon = \varepsilon_{out} - \varepsilon_{in} \tag{6}$$

where ρ_{lin}, ρ_{lout}, ρ_{gin} and ρ_{gout} are the liquid and vapor densities evaluated at the inlet and outlet of the test section while x_{in} and x_{out}, e_{in} and e_{out}, ε_{in} and ε_{out} and γ_{in} and γ_{out} are the vapor quality, the entrained liquid fraction, the void fraction and the liquid droplet hold-up evaluated at the inlet and outlet of the test section.

The fraction of liquid entrained as droplets in the gas core e is estimated from a correlation proposed by Oliemans et al. (1986):

$$\frac{e}{1-e} = 10^{b_0}\rho_l^{b_1}\rho_g^{b_2}\mu_l^{b_3}\mu_g^{b_4}\sigma^{b_5}d^{b_6}J_l^{b_7}J_g^{b_8}g^{b_9} \tag{7}$$

where J_l and J_g are the superficial liquid and gas velocities:

$$J_l = \frac{(1-x)G}{\rho_l}, \quad J_g = \frac{xG}{\rho_g} \tag{8}$$

The exponents b_0–b_9 appearing in Eq. (7) are summarized in Table 4 as a function of the liquid film Reynolds number, which is defined as follows:

$$\mathrm{Re}_{lf} = (1-e)(1-x)\frac{Gd}{\mu_l} \tag{9}$$

A constraint to the values of the exponents b_0–b_9 in Eq. (7) is that the right-hand side of Eq. (7) forms a dimensionless group. As can be seen in Eq. (9), the liquid film Reynolds number depends on the fraction of liquid entrained e, so that an iterative calculation is required. Operatively, a first order estimate for e is obtained using the values b_0–b_9 from Table 4 which are applicable irrespective of the liquid film Reynolds number. The Reynolds number of the liquid film can then be calculated, and the estimate for e accordingly refined. The procedure is then repeated, with 2–3 steps typically required to converge.

The void fraction ε is predicted according to the expression of Woldesemayat and Ghajar (2007):

$$\varepsilon = J_g \Bigg/ \left\{ J_g\left[1 + \left(\frac{J_l}{J_g}\right)^{\left(\frac{\rho_g}{\rho_l}\right)^{0.1}}\right] + 2.9\left[\frac{gd\sigma(1+\cos\theta)(\rho_l-\rho_g)}{\rho_l^2}\right]^{0.25} \times (1.22 + 1.22\sin\theta)^{\frac{P_{atm}}{P}} \right\} \tag{10}$$

where the numerical constant 2.9 appearing in Eq. (10) has the dimension $\mathrm{m}^{-0.25}$, P_{atm} is atmospheric pressure and P is the system pressure.

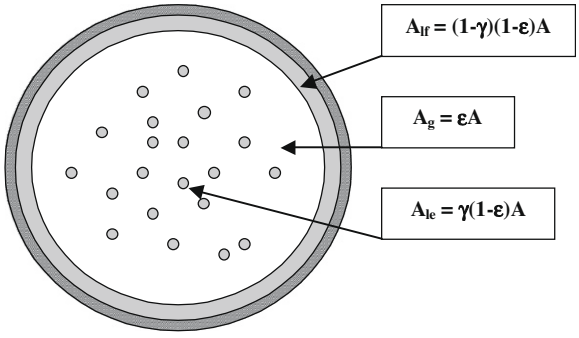

Fig. 3. Schematic representation of the cross sectional area A split among the phases.

Finally, the liquid droplet hold-up is estimated neglecting the slip between the entrained liquid droplets and the carrier gas phase as follows:

$$\gamma = e\frac{\varepsilon}{1-\varepsilon}\frac{1-x}{x}\frac{\rho_g}{\rho_l} \tag{11}$$

As can be seen, the estimate of the frictional pressure gradient in Eq. (2) depends on the liquid entrained fraction e and on the void fraction ε. Since the currently available predictive tools for these flow parameters are limited in validity to macroscale channels, the application of these methods to the data for microchannels should be considered as a first approximation.

According to Eq. (2), the frictional component of the total pressure gradient is predicted to be predominant over the accelerative and gravitational components in most of the data. The acceleration pressure gradient is typically a few percent of the total pressure gradient, while the gravitational component, which disappears for all the microscale data taken with horizontal test sections, is normally within 10–20% of the total but can reach up to 40–60% of the total in a few selected points characterized by low mass flux values.

The frictional component of the total pressure gradient estimated with Eq. (2) is compared with the correlation predictions in Figs. 12–16 and 18–24 in the Electronic Annex 2 in the online version of this article. The statistical comparisons between the measured data and predictions are reported in Tables 2 and 3 for the macroscale and microscale data, respectively. From inspection of Table 2 it can be seen that with macroscale data the best predictions are given by the correlation of Lombardi, with a mean absolute percentage error of 15.9% and 9 points out of 10 predicted to within ±30%, followed by the correlations of Friedel, Baroczy-Chisholm and the homogeneous model with the two-phase viscosity defined according to Cicchitti, Owens and Awad and Muzychka (definition No. 1 in Table a1 in the Electronic Annex 1 in the online version of this article).

From Table 3 with microscale data, the best predictions are still given by the correlation of Lombardi, with a mean absolute percentage error of 18.2% and 9 points out of 10 predicted to within ±30%, followed by the correlation of Müller-Steinhagen and Heck, the homogeneous model with the two-phase viscosity defined according to Cicchitti and Awad and Muzychka (definition No. 1 in Table a1 in the Electronic Annex 1 in the online version of this article) and the correlation of Friedel. Among the correlations considered here that are specifically designed for microchannels, the best performing one is the correlation of Sun and Mishima.

Good microscale predictions with the correlation of Müller-Steinhagen and Heck have been reported by Ribatski et al. (2006) and by Revellin and Thome (2007).

Since the homogeneous model is based on neglecting the slip between the phases, in principle it should be most effective for two-phase flows characterized by a fine mixing of the phases, such as bubbly flow and mist flow, while less effective whenever the phases tend to become segregated and consequently develop a slip, as happens with annular flow. Nonetheless, as can be seen in Tables 2 and 3, the homogeneous model can handle annular flow quite well, provided that the two-phase viscosity is properly defined. Within the limits of the present study, the best definitions of the two-phase viscosity for macroscale data are those proposed by Cicchitti and by Owens, in analogy with what was already observed by Idsinga et al. (1977), while for microscale data the best definitions of the two-phase viscosity are those proposed by Cicchitti and by Awad and Muzychka (definition No. 1 in Table a1 in the Electronic Annex 1 in the online version of this article).

Interestingly, the correlation of Lombardi works very well (taking the ±30% interval) for both the macroscale and the microscale databases, predicting correctly 89.4% of the former and 87.5% of the latter, using a criterion based on modified Bond and Weber number values to choose between two friction factor expressions.

5. Dimensional analysis and new prediction method

In what follows, a new correlating approach for the frictional pressure gradient based on dimensional analysis and capable of providing more physical insight than is typical of simple empirical correlations is proposed. In particular, a technique based on regression analysis and similar to that used by Stephan and Abdelsalam (1980) for natural convection boiling is used here.

In single-phase turbulent smooth pipe flow, the wall shear stress τ_w is assumed to depend on the fluid density ρ and viscosity μ, on the mean flow velocity V and on the tube diameter d as follows:

$$\tau_w = \tau_w(\rho, \mu, V, d) \tag{12}$$

As it is well known, the application of dimensional analysis to Eq. (12) relates the Fanning friction factor f to the Reynolds number as follows:

$$f = \frac{\tau_w}{\frac{1}{2}\rho V^2} = f\left(\frac{\rho V d}{\mu}\right) \tag{13}$$

This approach can be extended to annular two-phase flow assuming the wall shear stress τ_w to depend on the densities ρ_l and ρ_c and viscosities μ_l and μ_c of the liquid and the droplet-laden gas core, on the surface tension σ, on the mean velocities of the liquid film V_l and gas core V_c, on the gas core hydraulic diameter d_c and on the average liquid film thickness t as follows:

$$\tau_w = \tau_w(\rho_l, \rho_c, \mu_l, \mu_c, \sigma, V_l, V_c, d_c, t) \tag{14}$$

In a first approximation, an annular flow can be considered to consist of a liquid film single-phase flow plus a spray flow (gas and entrained droplets), where the spray flow can be treated as an equivalent single-phase flow. An annular flow, therefore, can be ideally decomposed in two single-phase flows, flowing concurrently through the channel. Since in single-phase channel flow the density ρ, the viscosity μ, the mean flow velocity V and a characteristic dimension of the flow d do the job, as indicated in Eq. (12), it seems reasonable to assume as influential parameters the densities ρ_l and ρ_c, the viscosities μ_l and μ_c, two mean flow velocities V_l and V_c and two characteristic dimensions, which are assumed to be the

Table 4
Parameters for Oliemans et al. correlation.

Re_{lf}	b_0	b_1	b_2	b_3	b_4	b_5	b_6	b_7	b_8	b_9
All values	−2.52	1.08	0.18	0.27	0.28	−1.80	1.72	0.70	1.44	0.46
10^2–3×10^2	−0.69	0.63	0.96	−0.80	0.09	−0.88	2.45	0.91	−0.16	0.86
3×10^2–10^3	−1.73	0.94	0.62	−0.63	0.50	−1.42	2.04	1.05	0.96	0.48
10^3–3×10^3	−3.31	1.15	0.40	−1.02	0.46	−1.00	1.97	0.95	0.78	0.41
3×10^3–10^4	−8.27	0.77	0.71	−0.13	−1.18	−0.17	1.16	0.83	1.45	−0.32
10^4–3×10^4	−6.38	0.89	0.70	−0.17	−0.55	−0.87	1.67	1.04	1.27	0.07
3×10^4–10^5	−0.12	0.45	0.25	0.86	−0.05	−1.51	0.91	1.08	0.71	0.21

average liquid film thickness t for the liquid film flow and the core diameter d_c for the core flow. In other words, ρ_l, μ_l, V_l and t are assumed to characterize the liquid film single-phase flow, while ρ_c, μ_c, V_c and d_c are assumed to characterize the core flow (gas plus entrained droplets). Surface tension σ is further included since it governs the interaction between the liquid film and the gas core, as extensively demonstrated in the literature. These considerations detail the reasoning behind Eq. (14).

This list of influential parameters in Eq. (14) is not claimed or expected to be complete but should, nonetheless, include all the essential physical properties that influence the wall shear stress in annular two-phase flow. The mean velocities of the liquid film V_l and gas core V_c are calculated as follows:

$$V_l = \frac{(1-e)(1-x)\Gamma}{\pi\rho_l t(d-t)}, \quad V_c = \frac{4}{\pi}\frac{[x+e(1-x)]\Gamma}{\rho_c d_c^2} \tag{15}$$

where e is the fraction of liquid entrained as droplets in the gas core, estimated with Oliemans et al. (1986) correlation, Eq. (7), while Γ is the total mass flow rate. The average liquid film thickness t is estimated by numerically integrating the mass conservation equation for the liquid film:

$$(1-e)(1-x)\Gamma = 2\pi\rho_l\int_0^t V_{lf}(y)(R-y)dy \tag{16}$$

where R and y are the tube radius and the distance from the tube wall, respectively, while the velocity profile in the liquid film V_{lf} is estimated according to Cioncolini et al. (2009) as follows:

$$V_{lf}^+ = \frac{1}{\in_{lf}^+}\left\{\frac{1}{1-\xi}\left[y^+ - \frac{y^{+2}}{2R^+} + \xi R^+\ln\left(1-\frac{y^+}{R^+}\right)\right] + \frac{1}{2}C_{lf}y^{+2}\right\}, \quad 0 \leqslant y^+ \leqslant t^+ \tag{17}$$

$$\xi = \frac{x^2G^2}{\varepsilon}\left|\frac{dv_g}{dP}\right|, \quad C_{lf} = \frac{y^{*2}}{\mu_l V^*}\left(\rho_l - \frac{\rho_l(1-\varepsilon)+\rho_g\varepsilon}{1-\xi}\right)g\sin\theta, \quad \in_{lf}^+ = \sqrt{1+0.90\cdot 10^{-3}t^{+2}} \tag{18}$$

where v_g is the gas phase specific volume and P the pressure. The dimensionless variables appearing in Eq. (17), together with the velocity V^* and length y^* scales, are defined as follows:

$$V_{lf}^+ = \frac{V_{lf}}{V^*}, \quad y^+ = \frac{y}{y^*}, \quad R^+ = \frac{R}{y^*}, \quad t^+ = \frac{t}{y^*}, \quad V^* = \sqrt{\frac{\tau_w}{\rho_l}}, \quad y^* = \frac{\mu_l}{\rho_l V^*} \tag{19}$$

Once the average liquid film thickness t is known, the core flow diameter is simply calculated as $d_c = d - 2t$, while the void fraction ε and the liquid droplet hold-up γ can be calculated from the following relations:

$$(1-\varepsilon)(1-\gamma) = \frac{t(2R-t)}{R^2}, \quad \gamma\frac{1-\varepsilon}{\varepsilon} = e\frac{1-x}{x}\frac{\rho_g}{\rho_l} \tag{20}$$

where the left expression is derived from the liquid film flow area, while that on the right is derived by neglecting the slip between the carrier gas and the entrained droplets. It is worth noting that the above outlined procedure could be reversed: the void fraction could be estimated from an empirical correlation, such as Eq. (10), and the liquid droplet hold-up could then be calculated neglecting the slip between the carrier gas and the entrained droplets, Eq. (11), and finally the average liquid film thickness could be calculated from the void fraction and liquid droplet hold-up values. Estimating the average liquid film thickness from integrating the liquid film velocity profile, however, was found to be more accurate and therefore was preferred in the present analysis. Finally, the density ρ_c and the viscosity μ_c of the droplet-laden gas core are calculated as follows:

$$\rho_c = (1-\varepsilon_c)\rho_l + \varepsilon_c\rho_g, \quad \mu_c = (1-\varepsilon_c)\mu_l + \varepsilon_c\mu_g \tag{21}$$

where ε_c is the droplet laden gas core void fraction and is calculated as:

$$\varepsilon_c = \frac{\varepsilon}{\varepsilon+\gamma(1-\varepsilon)} \tag{22}$$

Returning to Eq. (14), application of dimensional analysis relates the two-phase Fanning friction factor f_{tp} to the six dimensionless groups Π_1–Π_6 as follows:

$$f_{tp} = \frac{\tau_w}{\frac{1}{2}\rho_c V_c^2} = f_{tp}(\Pi_1, \Pi_2, \ldots, \Pi_6) \tag{23}$$

$$\Pi_1 = \frac{\rho_l}{\rho_c}, \quad \Pi_2 = \frac{\mu_l}{\mu_c}, \quad \Pi_3 = \frac{\rho_c V_c d_c}{\mu_c} = \mathrm{Re}_c, \quad \Pi_4 = \frac{\rho_l V_l d_l}{\mu_l} = \mathrm{Re}_l$$
$$\Pi_5 = \frac{\rho_c V_c^2 d_c}{\sigma} = We_c, \quad \Pi_6 = \frac{t}{d_c} \tag{24}$$

The liquid film hydraulic diameter d_l is calculated as:

$$d_l = 4\frac{t}{d}(d-t) \tag{25}$$

A detailed derivation of the dimensionless groups Π_1–Π_6 is included in the Appendix A. As can be seen, Π_1 and Π_2 are the ratios of the densities and viscosities of the liquid film and the gas core, respectively, Π_3 is a Reynolds number of the gas core, Π_4 is a Reynolds number of the liquid film, Π_5 is a Weber number for the gas core and Π_6 is the dimensionless liquid film thickness. Although the dimensionless groups Π_1–Π_6 are among the most frequently used in the annular two-phase flow literature, it is worth noting that several other groups might be generated through manipulation of the equations. Thus, returning to Eq. (23), one possible form is a power law representation:

$$f_{tp} = \frac{\tau_w}{\frac{1}{2}\rho_c V_c^2} = f_{tp}(\Pi_1, \Pi_2, \ldots, \Pi_6) = C\cdot\Pi_1^{a_1}\Pi_2^{a_2}\Pi_3^{a_3}\Pi_4^{a_4}\Pi_5^{a_5}\Pi_6^{a_6} \tag{26}$$

Power law representations have proved to be appropriate in many engineering applications, so that even though assuming a power law representation is rather arbitrary, nonetheless it can be considered an acceptable starting point. Besides, a power law representation allows the use of multiple regression analysis to both fix the values of the constant C and exponents a_i that best fit the data and to provide a ranking of importance of the groups Π_1–Π_6, allowing selection of those groups that exert the most significant influence on the friction factor f_{tp}. Since dimensional analysis is being applied here to provide physical insight, the possibility of reducing the number of dimensionless groups while keeping the most influential ones is believed to be of considerable importance. The ranking of the groups Π_1–Π_6 is achieved in different steps according to the following scheme. In the first step, equations of the following form are assumed, one for each group Π_i:

$$f_i^{step1} = C\cdot\Pi_i^{a_i}, \quad i = 1,\ldots,6 \tag{27}$$

For each Π_i, the constant C and the exponent a_i are calculated from fitting the experimental data with the least square method, while the square error sum is calculated as indicated in Eq. (28), where the sum spans the entire database.

$$Q_i^{step1} = \sum(f_{tp} - f_i^{step1})^2, \quad i = 1,\ldots,6 \tag{28}$$

The smallest square error sum allows the identification of the most influential group Π_i among Π_1–Π_6. In the second step, equations of the following form are assumed for the remaining groups Π_i:

Table 5
Range of dimensionless groups.

	Macroscale	Microscale
ρ_l/ρ_c	1.75–817	18.5–146
μ_l/μ_c	1.55–54.9	11.5–38.5
Re_c	1.2×10^4–4.6×10^6	6.7×10^3–8.5×10^4
Re_l	2.7×10^1–1.2×10^5	3.6×10^1–6.3×10^3
We_c	3.5×10^1–3.4×10^5	6.8×10^1–3.6×10^3
t/d_c	5.2×10^{-5}–2.6×10^{-1}	6.9×10^{-3}–1.7×10^{-1}

$$f_i^{step2} = C\cdot\Pi^b\cdot\Pi_i^{a_i},\quad i=1,\ldots,5 \tag{29}$$

where Π^b stands for the most influential group identified in the first step of the analysis. For each of the remaining Π_i, the constant C and the exponent a_i are calculated from fitting the experimental data with the least square method, while the identification of the smallest square error sum allows the selection of the second most influential group Π_i. The procedure is repeated until all groups are ranked. Examination of the evolution of the square error sums through the successive steps of regression analysis demonstrates when the inclusion of a further group no longer provides any appreciable increase in accuracy.

As can be seen, the analysis outlined so far strongly depends on the predictions of the entrained liquid fraction and of the velocity profile in the liquid film. Since the currently available predictive tools for these key parameters are limited in validity to macroscale channels, the analysis presented above is applied to the present macroscale experimental data only. Since all these macroscale data refer to vertical upflow, the cylindrical symmetry of the flow that has been tacitly assumed thus far is appropriate. The ranking of the dimensionless groups Π_1–Π_6 in diminishing order of importance is: We_c, μ_l/μ_c, Re_c, t/d_c, Re_l, ρ_l/ρ_c. The ranges that the dimensionless groups Π_1–Π_6 cover in the present study are summarized in Table 5. Significantly, inclusion of more than one dimensionless group beyond We_c was found to yield a negligible gain in accuracy, so that the final form of Eq. (26) that fits the present macroscale experimental database is the following:

$$f_{tp} = 0.172We_c^{-0.372} \tag{30}$$

The two-phase Fanning friction factor and the gas core Weber number values are displayed in Fig. 4, demonstrating that Eq. (30) fits the data reasonably well.

The application of dimensional analysis to the macroscale annular flow database, therefore, identifies the droplet-laden gas core Weber number as the most influential dimensionless group in determining annular flow shear stress and the corresponding frictional pressure gradient. As such, within the limits of the present analysis, friction in adiabatic annular two-phase flow seems to be mostly determined by the inertia of the droplet-laden gas core and by the surface energy of the interface between the liquid film and the gas core. Of critical importance, therefore, are the fraction of liquid entrained as droplets in the gas core, which directly affects the gas core inertia, and the morphology of the interface between the liquid film and the gas core.

It might be surprising that a single dimensionless group, We_c, correlates all of the data and hence some physical interpretation may explain why. The interpretation of the Weber number as a ratio of forces is helpful but might be somewhat limited, due to the large number of comparable dynamic forces that influence the hydrodynamics of annular flows and the feedbacks existing among them. The Weber number is typically used in the analysis of multiphase flows characterized by an interface separating two different fluids. In particular, the Weber number is a controlling dimensionless group in spray theory in general, in the study of liquid atomization and in the study of surface tension waves on shear-driven liquid films. In annular two-phase flow, the core flow can be considered as a spray interacting with the liquid film, which is shear-driven by the core flow and characterized by surface tension waves appearing at its surface. The tips of such waves are atomized by the core flow, giving rise to the entrainment. As such, the emergence of the Weber number as a characterizing group for annular flows appears consistent with annular flow phenomena. The empirical correlation of Lombardi (Lombardi and Carsana, 1992), which is the best performing correlation among the ones considered in the present study, is also based on a different type of modified Weber number to correlate the two-phase friction factor.

The insight provided by Eq. (30) can also be of interest in the context of proper selection of a two-phase flow experimental test matrix, where the behavior of a two-phase flow system is investigated on reduced-scale test facilities. If the natural circulation rate of the system is of interest, as frequently happens with nuclear system testing for safety applications, friction-preserving scaling of the system piping becomes crucial and the information provided by Eq. (30) can prove useful for a proper scaling of the piping subject to annular flow.

Although the turbulence structure in shear-driven liquid films is not yet completely clarified, it is commonly accepted that thick

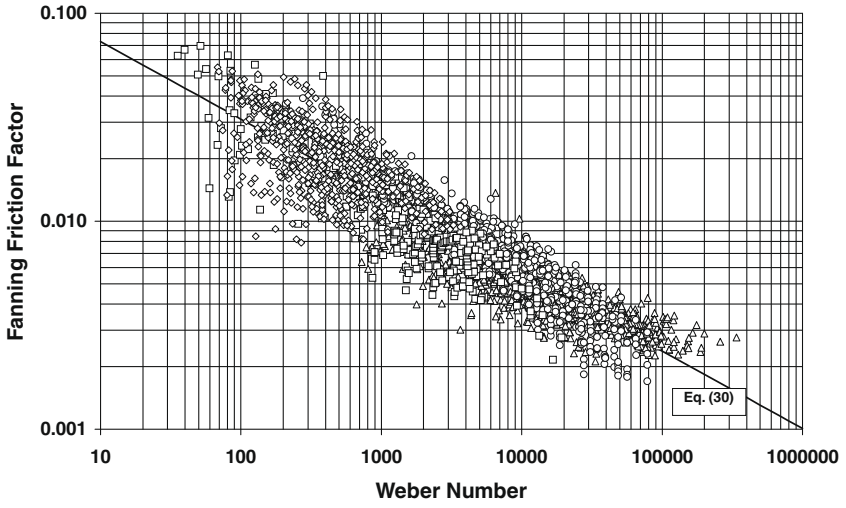

Fig. 4. Core flow Fanning friction factor vs. core flow Weber number.

films should be mostly turbulent, while laminarization should be observed in very thin films. The average liquid film thickness values predicted from integration of Eq. (16) are in the range of 10^{-6}–10^{-3} m, corresponding to a 10–1000 range for the dimensionless thickness t^+. As such, both laminar and turbulent liquid films should be covered in the present macroscale study.

Statistically, Eq. (30) fits the data well enough to attempt to use it to predict the pressure gradient in practical applications. In this respect, the two-phase total pressure gradient can be predicted as follows:

$$-\left(\frac{dP}{dz}\right)_{tpf-t} = 2f_{tp}\frac{G_c^2}{\rho_c d} + G^2\frac{d}{dz}\left[\frac{x^2}{\rho_g\varepsilon} + \frac{e^2(1-x)^2}{\rho_l\gamma(1-\varepsilon)} + \frac{(1-e)^2(1-x)^2}{\rho_l(1-\gamma)(1-\varepsilon)}\right] + [\rho_l(1-\varepsilon)+\rho_g\varepsilon]g\sin(\theta) \quad (31)$$

where the two-phase Fanning friction factor f_{tp} is provided by Eq. (30). In principle, the value of the average liquid film thickness that is required as input to Eq. (30) should be obtained from integration of the liquid film velocity profile, as indicated in Eq. (16). In order to make the use of Eq. (31) easier for engineering applications, however, the average liquid film thickness t and the core flow diameter d_c can be predicted from the void fraction ε and the liquid droplet hold-up γ values as follows:

$$t \approx \frac{d}{2}\left(1-\sqrt{\varepsilon+\gamma-\varepsilon\gamma}\right), \quad d_c \approx d\sqrt{\varepsilon+\gamma-\varepsilon\gamma} \quad (32)$$

where the void fraction ε is predicted according to Woldesemayat and Ghajar (2007), Eq. (10) and the liquid droplet hold-up γ is calculated neglecting the slip between entrained droplets and carrier gas phase, Eq. (11). The core flow mass flux G_c and Weber number We_c can correspondingly be estimated as follows.

$$G_c = \frac{4}{\pi}\frac{[x+e(1-x)]\Gamma}{d_c^2}, \quad We_c = \frac{G_c^2 d_c}{\rho_c\sigma} \quad (33)$$

where the liquid entrained fraction e is predicted according to Oliemans et al. (1986), Eq. (7) and the core flow density ρ_c is calculated according with Eqs. (21) and (22). Since both G_c and We_c depend on $d_c = (d-2t)$ and since d is generally much bigger than t, even a rough estimate of the average liquid film thickness provides a reasonably accurate prediction of the core mass flux and Weber number. This conclusion is, however, limited to these two parameters, and in the context of the complete dimensional analysis the average liquid film thickness is more accurately estimated from integrating the velocity profile in the liquid film, as already discussed. As can be seen, although Eq. (30) is very simple, the actual calculation of the core flow Weber number required to use it is a bit more involved.

The results are presented in Fig. 5, where the measured total pressure gradient values are displayed versus the predictions of Eq. (31). From inspection of Fig. 5, a systematic overprediction of very low pressure gradient values obtained with water–air flows can be noticed. Besides having large experimental uncertainties, due to the very small pressure drop values measured, these very low pressure gradient points are further characterized by a predominance of the gravitational component of the total pressure gradient. As such, accurately predicting the void fraction becomes crucial, while the wall shear stress backed out of the calculation becomes quite inaccurate.

In Table 2 it can be seen that Eq. (31) fits the macroscale data better than all the other correlations tested, with a mean absolute percentage error of 13.1% and 7 out of 10 points predicted to within ±15%. Direct comparison of Eq. (31) with other correlations, however, is somewhat unfair, since Eq. (31) is based on the present data set while all other correlations have been designed with different experimental data banks. Nonetheless, the good performance of Eq. (31) further suggests that, within the limits of the present study, the core flow Weber number seems to be the best parameter to capture the essence of friction in adiabatic annular two-phase flow.

Although not used to develop Eq. (30), the present microscale experimental data are nonetheless included in Fig. 4 for comparison. The microscale points cluster quite well, suggesting that the present approach may work for microchannels as well, provided that dedicated design tools to predict the liquid entrained fraction and the velocity profile in the liquid film become available (the macroscale methods have been applied here). Besides, although derived by fitting macroscale data only, Eq. (30) provides an acceptable fit of microscale data as well, suggesting that the present macroscale approach can be extrapolated, in first approximation, to microchannels. The microscale two-phase total pressure gradient can then be predicted with Eqs. (30) and (31), and the results are presented in Fig. 6, where the measured total pressure gradient values are displayed versus the predicted ones. Table 3 shows that the macroscale method proposed here, Eqs. (30) and (31), extrapolates reasonably well to microchannels, yielding a mean absolute percentage error of 28.8% that is comparable with the errors of the correlation of Friedel and of the microscale method of Sun and Mishima. Future work should concentrate on measurement of the liquid entrained fraction and of the velocity

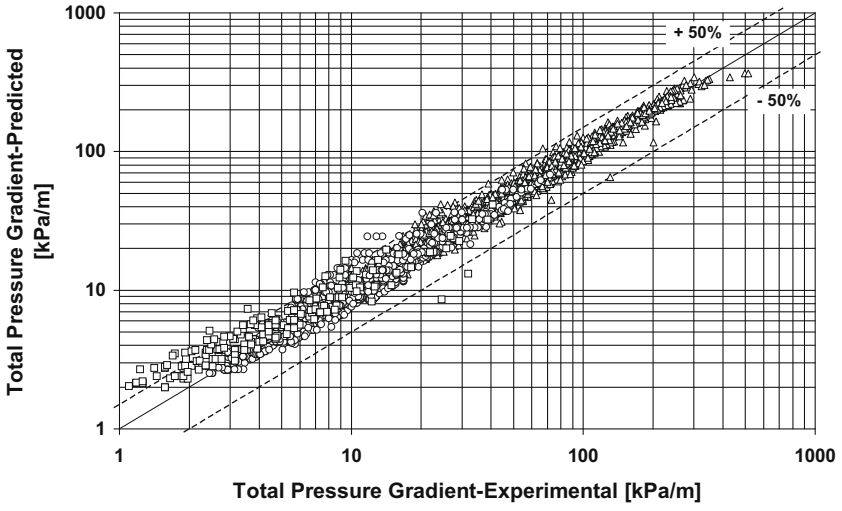

Fig. 5. Total pressure gradient: predicted with Eqs. (30) and (31) vs. measured macroscale data.

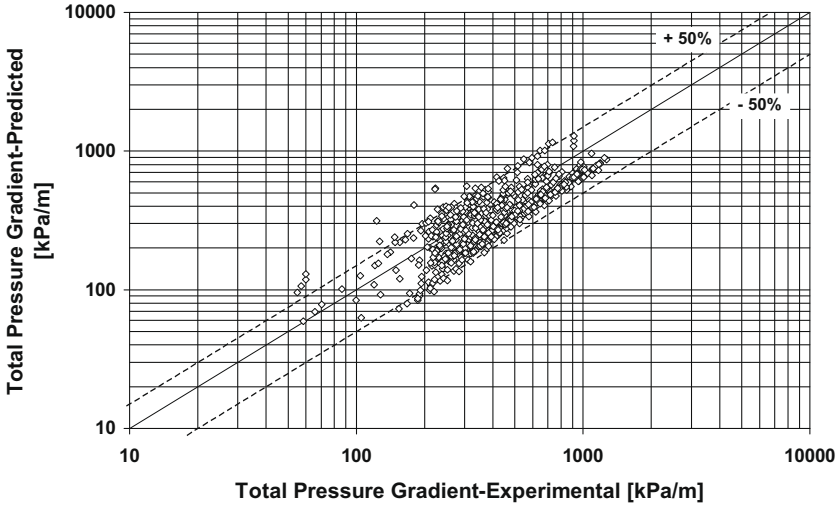

Fig. 6. Total pressure gradient: predicted with Eqs. (30) and (31) vs. measured microscale data.

profile in the liquid film in microscale tests. For the time being, more accurate microscale predictions for use in engineering applications can be obtained if the two-phase Fanning friction factor, instead of being predicted with Eq. (30), is calculated as follows:

$$f_{tp-\mu} = 0.0196 We_c^{-0.372} Re_l^{0.318} \tag{34}$$

where the liquid film Reynolds number Re_l is calculated as:

$$Re_l = (1-e)(1-x)\frac{Gd}{\mu_l} \tag{35}$$

Eq. (34) is derived from Eq. (30) by including an empirical correction based on the liquid film Reynolds number Re_l that is optimized with the present microscale database. Within the limits of the present study, the inclusion of the liquid film Reynolds number in the correlating equation of the two-phase Fanning friction factor is apparently capable of compensating for the already highlighted deficiencies of the macroscale methods that are extrapolated here down to microchannels to predict the liquid entrained fraction and the velocity profile in the liquid film. The results are presented in Fig. 7, where the measured total pressure gradient values are displayed versus the predictions of Eqs. (31) and (34). In Table 3 it can be seen that Eqs. (31) and (34) fit the microscale data better than all the other correlations tested, with a mean absolute percentage error of 13.1% and almost all points predicted to within ±30%.

For practical applications, the selection between Eqs. (30) and (34) to predict the two-phase Fanning friction factor should be done according to the value of the Bond number defined here as:

$$Bo = \frac{g(\rho_l - \rho_g)d^2}{\sigma} \tag{36}$$

As suggested by Kew and Cornwell (1997), the macro-to-microscale transition occurs at $Bo \approx 4$, with values below 4 being in the microscale. Accordingly, Eq. (30) should be used for Bond number values above 4, while Eq. (34) should be used for Bond number values below 4.The Bond number range covered in the present macroscale database is 7.8–208, while microscale data cover the range of 0.25–1.6.

6. Conclusions

The performances of 24 empirical correlations for use in predicting two-phase flow pressure drops were evaluated with respect to experimental data for annular two-phase flow. Within

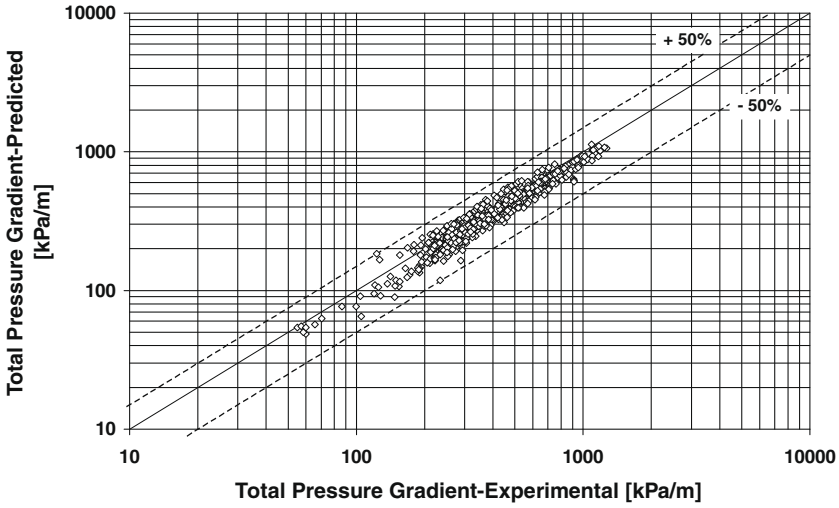

Fig. 7. Total pressure gradient: predicted with Eqs. (31) and (34) vs. measured microscale data.

the limits of the present study, for both microscale and macroscale data, the best predictions by an existing method are given by far by the correlation of Lombardi.

Applying dimensional analysis on annular two-phase flow, and using only macroscale annular flow data, the Weber number of the droplet laden gas core was found to be the lone dominant dimensionless group. It has the benefit of including intrinsically the effects of the gas core velocity, the entrained liquid fraction and the average liquid film thickness, thus providing more physical insight into the two-phase frictional pressure gradient than other previous correlations. The new gas core Weber number based correlation proposed here gave the best predictions for the macroscale database and yielded encouraging results when extrapolated to the microscale database, suggesting that the gas core Weber number may be the lone dominant dimensionless group in the microscale as well. The new gas core Weber number based correlation proposed here was modified to improve its predictive capability with microchannels.

Acknowledgement

A. Cioncolini is supported by Swiss National Fund (SNF) Contract No. 200020-119651.

Appendix A

Starting from Eq. (14), ρ_c, V_c and d_c are chosen to derive the intrinsic scales for measuring mass, length and time:

$$[M] = \rho_c d_c^3 \tag{A1}$$

$$[L] = d_c \tag{A2}$$

$$[t] = d_c V_c^{-1} \tag{A3}$$

The set of dimensionless groups that is correspondingly obtained is as follows:

$$\Pi_1 = \frac{\rho_l}{\rho_c}, \quad \Pi_2 = \frac{\mu_l}{\rho_c V_c d_c}, \quad \Pi_3 = \frac{\mu_c}{\rho_c V_c d_c}, \quad \Pi_4 = \frac{V_l}{V_c},$$
$$\Pi_5 = \frac{\sigma}{\rho_c V_c^2 d_c}, \quad \Pi_6 = \frac{t}{d_c} \tag{A4}$$

In dimensional analysis, it is common practice to manipulate the dimensionless groups in order to facilitate their physical interpretation and/or better capture the features of the phenomenon under investigation. In particular, Π_2 is formally the inverse of a Reynolds number, but contains mixed parameters (some referring to the liquid, some referring to the core) that make its interpretation difficult. It is therefore manipulated as follows:

$$\Pi_2 \mapsto \Pi_2 \Pi_3^{-1} = \frac{\mu_l}{\mu_c} \tag{A5}$$

This form is preferred, since it is formally analogous to Π_1. For what concerns Π_3, it is the inverse of a core flow Reynolds number, so it is kept as it is, just inverted:

$$\Pi_3 \mapsto \Pi_3^{-1} \tag{A6}$$

Π_5 is the inverse of a core flow Weber number, so it is kept as it is, just inverted:

$$\Pi_5 \mapsto \Pi_5^{-1} \tag{A7}$$

Π_4 is the slip between the liquid film and the core flow (droplets and gas). Although it might be kept as it is, a different form was preferred. Inspecting the other dimensionless groups it can be seen that inertia in the core flow, viscous dissipation in the core flow and surface energy of the interface between film and core are already represented, but inertia and viscous dissipation in the liquid film are still missing. It was therefore preferred to manipulate Π_4 in order to get a Reynolds number for the liquid film:

$$\Pi_4 \mapsto \Pi_4 \Pi_1 \Pi_2^{-1} \Pi_3 \Pi_6 = \frac{\rho_l V_l t}{\mu_l} \tag{A8}$$

Π_4 is now a Reynolds number for the liquid film, with the average liquid film thickness t as characteristic dimension. Although it might be kept in this form, a further improvement was considered. The hydraulic diameter of the liquid film is as follows:

$$d_l = 4\frac{t}{d}(d-t) = 4t\frac{d_c + t}{d_c + 2t} \approx 4t \iff d \gg t \tag{A9}$$

As can be seen, the average liquid film thickness t is a good measure of the hydraulic diameter of the liquid film (apart from the multiplicative constant 4) only in the limit of very thin films. Since the experimental data bank used here is not limited to very thin films, the liquid film Reynolds number is modified by replacing the average liquid film thickness t with the liquid film hydraulic diameter:

$$\Pi_4 \mapsto \frac{\rho_l V_l d_l}{\mu_l} \tag{A10}$$

This kind of manipulation might be questioned. Since the available information is used as suggested by physical intuition, the manipulation looks legitimate: although dimensional analysis is a mathematical tool, it is applied to real-world problems, so that some flexibility is required. Besides, in the end, the influence of the liquid film Reynolds number turns out to be negligible. Physically-inspired modifications of dimensionless groups are not rare in two-phase flow. For example, Π_1 might be modified as follows:

$$\Pi_1 \mapsto \frac{\rho_l - \rho_c}{\rho_c} \tag{A11}$$

Some authors found this form of the density ratio more effective to capture huge pressure variations. In the present study, however, the density ratio was not modified as described above.

The set of dimensionless groups that is finally obtained is as indicated in Eq. (24).

Appendix B. Supplementary data

Supplementary data associated with this article can be found, in the online version, at doi:10.1016/j.ijmultiphaseflow.2009.07.005.

References

Adorni, N., Casagrande, I., Cravarolo, L., Hassid, A., Pedrocchi, E., Silvestri, M., 1963. Further investigations in adiabatic dispersed flow: pressure drop and film thickness measurements with different channel geometries-analysis of the influence of geometrical and physical parameters. CISE Report R-53.

Anderson, G.H., Mantzouranis, B.G., 1960. Two-phase (gas–liquid) flow phenomena – I: pressure drop and hold-up for two-phase flow in vertical tubes. Chem. Eng. Sci. 12, 109–126.

Awad, M.M., Muzychka, Y.S., 2008. Effective property models for homogeneous two-phase flows. Exp. Therm. Fluid Sci. 33, 106–113.

Baroczy, C.J., 1966. A systematic correlation for two-phase pressure drop. Chem. Eng. Prog. Symp. Ser. 62, 232–249.

Beattie, D.R.H., Whalley, P.B., 1982. Simple two-phase frictional pressure drop calculation method. Int. J. Multiphase Flow 8, 83–87.

Casagrande, I., Cravarolo, L., Hassid, A., Pedrocchi, E., 1963. Adiabatic dispersed two-phase flow: further results on the influence of physical properties on pressure drop and film thickness. CISE Report R-73.

Chisholm, D., 1973. Pressure drop due to friction during the flow of evaporating two-phase mixtures in smooth tubes and channels. Int. J. Heat Mass Transfer 16, 347–358.

Cicchitti, A., Lombardi, C., Silvestri, M., Soldaini, G., Zavattarelli, R., 1960. Two-phase cooling experiments – pressure drop, heat transfer and burnout experiments. Energia Nucleare 7, 407–425.

Cioncolini, A., Thome, J.R., Lombardi, C., 2009. Algebraic turbulence modeling in adiabatic gas–liquid annular two-phase flow. Int. J. Multiphase Flow 35, 580–596.

Consolini, L., 2008. Convective boiling heat transfer in a single micro-channel. Ph.D. Thesis, École Polytechnique Fédérale de Lausanne, Switzerland. Available at <http://library.epn.ch/en/theses/?nr=4024>.

Cravarolo, L., Hassid, A., Pedrocchi, E., 1964. Further investigation on two-phase adiabatic annular-dispersed flow: effect of length and some inlet conditions on flow parameters. CISE Report R-93.

Davidson, W.F., Hardie, P.H., Humphreys, C.G.R., Markson, A.A., Mumford, A.R., Ravese, T., 1943. Studies of heat transmission through boiler tubing at pressures from 500 to 3000 Lbs. Trans. ASME 65, 553–591.

Dukler, A.E., Wicks, M., Cleveland, R.G., 1964. Frictional pressure drop in two-phase flow, part A: a comparison of existing correlations for pressure loss and holdup and part B: an approach through similarity analysis. AIChE J. 10, 38–51.

Friedel, L., 1979. Improved friction pressure drop correlation for horizontal and vertical two-phase pipe flow. European Two-Phase Flow Group Meeting, paper E2, Ispra, Italy.

Garcia, F., Garcia, R., Padrino, J.C., Mata, C., Trallero, J.L., Joseph, D.D., 2003. Power law and composite power law friction factor correlations for laminar and turbulent gas–liquid flow in horizontal pipelines. Int. J. Multiphase Flow 29, 1605–1624.

Gaspari, G.P., Lombardi, C., Peterlongo, G., 1964. Pressure drops in steam–water mixtures. CISE Report R-83.

Gill, L.E., Hewitt, G.F., Lacey, P.M.C., 1964. Sampling probe studies of the gas core in annular two-phase flow – II: studies of the effect of phase flow rates on phase and velocity distribution. Chem. Eng. Sci. 19, 665–682.

Gill, L.E., Hewitt, G.F., Lacey, P.M.C., 1965. Data on the upwards annular flow of air–water mixtures. Chem. Eng. Sci. 20, 71–88.

Hewitt, G.F., Roberts, D.N., 1969. Studies of two-phase flow patterns by simultaneous X-ray and flash photography. AERE-M 2159, HMSO.

Idsinga, W., Todreas, N., Bowring, R., 1977. An assessment of two-phase pressure drop correlations for steam–water systems. Int. J. Multiphase Flow 3, 401–413.

Kandlikar, S.G., 2002. Fundamental issues related to flow boiling in minichannels and microchannels. Exp. Therm. Fluid Sci. 26, 389–407.

Kew, P., Cornwell, K., 1997. Correlations for prediction of boiling heat transfer in small diameter channels. Appl. Therm. Eng. 17, 705–715.

Lockhart, R.W., Martinelli, R.C., 1949. Proposed correlation of data for isothermal two-phase, two-component flow in pipes. Chem. Eng. Progr. 45, 39–48.

Lombardi, C., Carsana, C.G., 1992. A dimensionless pressure drop correlation for two-phase mixtures flowing upflow in vertical ducts covering wide parameter range. Heat Technol. 10, 125–141.

Martinelli, R.C., Nelson, D.B., 1948. Prediction of pressure drop during forced-circulation boiling of water. Trans. ASME 70, 695–702.

McAdams, W.H., Woods, W.K., Heroman, L.C., 1942. Vaporization inside horizontal tubes: II – benzene-oil mixtures. Trans. ASME 64, 193–200.

Mishima, K., Hibiki, T., 1996. Some characteristics of air-water two-phase flow in small diameter vertical tubes. Int. J. Multiphase Flow 22, 703–712.

Müller-Steinhagen, H., Heck, K., 1986. A simple friction pressure drop correlation for two-phase flow in pipes. Chem. Eng. Process. 20, 297–308.

Oliemans, R.V.A., Pots, B.F.M., Trompé, N., 1986. Modeling of annular dispersed two-phase flow in vertical pipes. Int. J. Multiphase Flow 12, 711–732.

Owens, W.L., 1961. Two-phase pressure gradient. ASME Int. Develop. Heat Transf. Part II 36, 3–368.

Revellin, R., 2005. Experimental two-phase fluid flow in microchannels. Ph.D. Thesis, École Polytechnique Fédérale de Lausanne, Switzerland. Available at <http://library.epn.ch/en/theses/?nr=3437>.

Revellin, R., Thome, J.R., 2007. Adiabatic two-phase frictional pressure drops in microchannels. Exp. Therm. Fluid Sci. 31, 673–685.

Ribatski, G., Wojtan, L., Thome, J.R., 2006. An analysis of experimental data and prediction methods for two-phase frictional pressure drop and flow boiling heat transfer in micro-scale channels. Exp. Therm. Fluid Sci. 31, 1–19.

Shannak, B.A., 2008. Frictional pressure drop of gas liquid two-phase flow in pipes. Nucl. Eng. Des. 238, 3277–3284.

Shearer, C.J., Nedderman, R.M., 1965. Pressure gradient and liquid film thickness in co-current upwards flow of gas/liquid mixtures: application to film cooler design. Chem. Eng. Sci. 20, 671–683.

Silvestri, M., Casagrande, I., Cravarolo, L., Hassid, A., Bertoletti, S., Lombardi, C., Peterlongo, G., Soldaini, G., Vella, G., Perona, G., Sesini, R., 1963. A research program in two-phase flow. CISE Report.

Stephan, K., 1992. Heat Transfer in Condensation and Boiling. Springer, Berlin.

Stephan, K., Abdelsalam, M., 1980. Heat-transfer correlations for natural convection boiling. Int. J. Heat Mass Transfer 23, 73–87.

Sun, L., Mishima, K., 2009. Evaluation analysis of prediction methods for two-phase flow pressure drop in mini-channels. Int. J. Multiphase Flow 35, 47–54.

Tran, T.N., Chyu, M.C., Wambsganss, M.W., France, D.M., 2000. Two-phase pressure drop of refrigerants during flow boiling in small channels: an experimental investigation and correlation development. Int. J. Multiphase Flow 26, 1739–1754.

Willis, I.J., 1965. Upwards annular two-phase air/water flow in vertical tubes. Chem. Eng. Sci. 20, 895–902.

Woldesemayat, M.A., Ghajar, A.J., 2007. Comparison of void fraction correlations for different flow patterns in horizontal and upward inclined pipes. Int. J. Multiphase Flow 33, 347–370.

Wolf, A., Jayanti, S., Hewitt, G.F., 2001. Flow development in vertical annular flow. Chem. Eng. Sci. 56, 3221–3235.

Zhang, W., 2006. Study on constitutive equations for boiling in mini-channels. Ph.D. Thesis, Kyoto University, Japan.